Philipp Ent 36 (2): 31-56 ISSN 0048-3753 July-December 2022

IN SILICO ANALYSIS OF *Peregrinus maidis* Ashmead SYNTAXIN 18 WITH MAIZE MOSAIC VIRUS GLYCOPROTEIN SUPPORTS NEUROTROPIC ROUTE BY WHICH THE VIRUS CAN SPREAD THROUGH THE INSECT VECTOR

Apel Jae Nayam-an Clemente and Karen Barandoc Alviar*

Institute of Weed Science, Entomology and Plant Pathology, College of Agriculture and Food Science, University of the Philippines Los Baños, College. 4031 Laguna, Philippines
*Corresponding author: kbalviar@up.edu.ph

ABSTRACT

The corn planthopper, *Peregrinus maidis* Ashmead (Hemiptera: Delphacidae), has been a constant problem in the corn production industry as it is a vector of two plant pathogenic viruses, *Maize mosaic virus* (MMV) and *Maize stripe virus* (MStV). MMV infection and intercellular dissemination in the vector may rely on the interaction of the t-SNARE Syntaxin-18 of *P. maidis* (PmStx18) which is a putative receptor for MMV glycoprotein (MMV G). To investigate this, functional annotation of PmStx18 and MMV G was performed in this study to come up with a reliable model for PmStx18—MMV G interaction through the utilization of bioinformatics tools. Analysis and protein-protein interaction (PPI) prediction used sequence-based and structure-based approaches. Results showed that the four best predicted docked complexes have 45, 42, 22 and 27 interacting residues with binding affinities (change in Gibbs free energy, ΔG) of -57.73, -57.05, -52.55, and -51.69, respectively, suggesting strong interactions. This *in silico* analysis performed for the interaction on a putative receptor of *P. maidis* and MMV G showed potential basis for constructing a double stranded RNA target for alternative pest management tool using RNA interference technology.

Key words: corn planthopper, *in silico* analysis, *Maize mosaica lphanucleorhabdovirus*, protein-protein interaction, Syntaxin 18

INTRODUCTION

Maize or corn (*Zea mays* L.) is a highly significant crop cultivated worldwide. It is a primary source of feeds and a food crop in Latin America, Sub-Saharan Africa, and Southeast Asia supplying an energy density of 365 Kcal/100g (Erenstein et al., 2022); (Ranum et al., 2014). It is also the second

most widely grown crop annually cultivated on an estimated 197 M hectares of land, in totality, with United States as the top maize producing country and contributor of 35% to the 967 million metric tons of total world maize production (Erenstein et al., 2022); Shah et al., 2016).

Annual crop losses of over USD 60 billion are attributed to plant viruses, that in 2012, significant economic losses amounted to USD 8 billion in maize yield (Abbas et al., 2022). Furthermore, from 2016 to 2019, an estimated mean economic loss of US$ 138.18 per hectare was due to reduced yield caused by maize diseases in the US and Ontario (Mueller et al., 2020).

The *Maize mosaic alphanucleorhabdovirus* (MMV) is one of the three primary tropical viruses of corn, along with *Maize streak virus* (MSV) and *Maize stripe virus* (MStV) (Abbas et al., 2022). Both MMV and MSV are transmitted by *Peregrinus maidis* (Ashmead), a planthopper vector of the Delphacidae family (Jourdan-Ruf et al., 1995). MMV replicates in *P. maidis* and high titers can be found in the nerve tissues of the insect (Hogenhout et al., 2008); Barandoc-Alviar et al., 2016).

MMV, now reclassified under the genus *Alphanucleorhabdovirus* (International Committee on Taxonomy of Viruses, 2020), causes maize mosaic disease which is characterized by stunting and regular chlorotic lines along the whole leaf length veins (Jourdan-Ruf et al., 1995). Here in the country, *P. maidis* devastation, evidenced by insect damage and visible MMV disease symptoms, is majorly observed among crops in surveyed corn fields of CALABARZON and Bicol region (K.B. Alviar, personal communication). MMV glycoprotein (MMV G) is implicated to be essential in the interaction with the insect host vector's cell receptors. MMV G is a trimer and a type I integral membrane protein consisting of ecto-transmembrane and cytoplasmic domains (Amaral et al., 2013; Weissenhorn et al., 2007; Hogenhout et al., 2003).

Syntaxin-18 is one of the identified MMV G-interacting proteins of *P. maidis* through high throughput membrane-based yeast two hybrid system (MbY2H) (Alviar et al., 2022 Preprint). It is a protein from the Syntaxin family under the soluble N-ethylmaleimide-sensitive factor-attachment protein receptor (SNARE) classification along with vesicle-associated membrane proteins (VAMPs) and synaptosomal-associated proteins (SNAPs) (Wang et al., 2017). SNARES are localized in the vesicle and target membranes and are significant for membrane fusion in the secretory and endocytic pathways (Yoon & Munson, 2018); Holz & Zimmerberg, 2019); (Hatsuzawa et al., 2000). Syntaxin-18, abbreviated hereon as Stx18, is specifically a target membrane SNARE (t-SNARE) protein (Bossis et al., 2005).

Protein-protein interaction (PPI) is the physical contact of two or more proteins and is the key to understand functions of unknown proteins (Farooq et al., 2021). Moreover, PPIs identification are performed in several studies utilizing sequence-based and structure-based *in silico* analyses, *in silico* two hybrid system, phylogenetic tree, phylogenetic profile and gene expression-based approaches that are found as online tools, software programs and servers available on the web to further discern the molecular basis virus-host relationship and interactions (Srinivasa Rao et al., 2014); Farooq et al., 2021). Here, we analyzed MMV G and PmStx18 protein structures and used *in silico* docking approach for the analysis of PPI between MMV G and PmStx18.

MATERIALS AND METHODS

PmStx18 dataset

The two DNA sequences of PmStx18 in FASTA format were opened using the Molecular Evolutionary Genetics Analysis X (MEGA-X) software program. The sequences were aligned using EMBOSS Needle (https://www.ebi.ac.uk/Tools/psa/). The length of the nucleotide sequence is 923 bp and 936 bp, respectively. The results showed 95.7% identity and similarity for the two sequences. The consensus sequence was generated, and homology search was performed in BLASTn (https://blast.ncbi.nlm.nih.gov/Blast.cgi), BLASTx (https://blast.ncbi.nlm.nih.gov/) and UniProtKB (https://www.uniprot.org/blast/). The sequence was run in three servers using default parameters. Protein translation was performed using Expasy translate (https://web.expasy.org/translate/). The resulting protein coding sequence was used for downstream analysis. The hydrophobicity of MMV G and PmStx18 proteins were calculated using ProtScale (https://web.expasy.org/protscale/).

Computational analysis and Functional annotation

Subsequent translation of the consensus sequence into protein was carried out using the Translate tool of ExPASy (https://web.expasy.org/translate/). From the resulting frames, the protein sequence of the identified open reading frame (ORF) was obtained. The physical and chemical characteristics of the amino acid sequence of the ORF region (GRAVY) was computed by the ProtParam tool (https://web.expasy.org/protparam/) of ExPASy. The presence of signal peptide on both proteins was predicted using the SignalP 5.0 server (http://www.cbs.dtu.dk/services/SignalP/). Furthermore, the protein sequences were submitted to InterPro (https://www.ebi.ac.uk/interpro/) for the prediction of the domains and were run using the default program.

Tertiary structures prediction, PPI prediction and analysis

The protein sequence of MMV G was retrieved from the protein database of NCBI (GenBank Accession No. QCS90261). Both the protein sequences of PmStx18 and the MMV G were submitted to I-TASSER (Iterative Threading Assembly Refinement) server found at https://zhanglab.dcmb.med.umich.edu/I-TASSER/ for the prediction tertiary structure as well as the binding sites. Default parameters were used.

For the analysis and prediction of interaction between MMV G and PmStx18, the top model for each protein was retrieved from I-TASSER. The best 3D models of PmStx18 and MMV G identified were submitted to HADDOCK 2.4 (https://wenmr.science.uu.nl/haddock2.4/) for the prediction of docked structure and properties. Default parameters were used. PmStx18—MMV G docked structure prediction was accomplished using the PyMOL Molecular Graphics System, version 2.5 (DeLano, Schrodinger, Inc.). This program was used in visualizing the docked structure as well as mapping and labelling the contact of interface residues of the complexes retrieved.

Binding affinities and pI prediction of interacting residues

Binding affinity ΔG (change in Gibbs free energy) and interacting residues were obtained from PRISM (http://cosbi.ku.edu.tr/prism/) web server. To calculate the isoelectric point of the interacting residues, the interacting amino acid sequences of two proteins in each predicted docked structure were submitted to ExPASy Compute pI/MW web server (https://web.expasy.org/compute_pi/) as well as in Isoelectric Point Calculator (http://isoelectric.ovh.org).

RESULTS AND DISCUSSION

The mosaic disease of corn is caused by *Maize mosaic alphanucleorhabdovirus* (MMV), a plant rhabdovirus which is transmitted by corn planthopper (*Peregrinus maidis*). The glycoprotein of MMV plays an important role in the acquisition, replication and transmission in host cells (both in plant and insect cells). MMV G is a trimeric and type I integral membrane protein with ecto-, transmembrane and cytosolic domains. Its fusion with cell membranes can be classified under Class III fusion membrane proteins (Backovic & Jardetzky, 2011; Weissenhorn et al., 2007).

Previous studies have identified the glycoprotein of plant and animal rhabdoviruses to be involved with host receptors as the initial step of viral

infection. The glycoprotein of animal-infecting rhabdoviruses such as rabies virus (RABV) and vesicular stomatitis virus (VSV) is the key protein involved in recognition of receptor and entry into cells (Roche et al., 2008; Yang et al., 2020). Moreover, according to Dietzgen et al. (2016), plant rhabdovirus glycoprotein spikes on viral surfaces are predicted to be interacting with receptors and entry into midgut epithelial cells through endocytosis. *In silico* analysis was utilized in this study to probe into the potential interaction of the t-SNARE *P. maidis* STX18 and MMV G since this could explain the mechanism of MMV entry, infection, and dissemination within the planthopper vector. The work of Castrosanto et al. (2022) performed the first *in silico* analysis for the insect vector's Stx18 interaction with MMV G. Here, we showed the MMV G and PmStx18 interacting ligands based in HADDOCK model prediction and the superimposed models of the proteins from their protein sequences and its closest homologues.

PmStx18 shows high similarity with closely related STX18 of plant- and leafhoppers and other hemipterans known as vectors of plant pathogens

Homologues retrieved from UniProtKB, BLASTx and BLASTn were summarizedin **Tables 1** and **2**, respectively. Homology search results from the three programs showed that the hits having the highest percent identity shared with PmStx18 are the STX18 of *Nilaparvata lugens* (80.74% from BLASTn and 64.76% in BLASTx) as well as *Laodelphax striatellus* (84.8% in UniProtKB and 63.44% in BLASTx). Moreover, there is 61.2% sequence similarity with *Blatella germanica*, 59.8% with *Thrips palmi*, 55.3% with *Frankliniella occidentalis*, and least similar with *Rhodnius prolixus* at 51.4%.

Table 1. Insect STX18 homologues retrieved from UniProtKB.

Hit	Gene	Organism	Score	E-value	Percent Identity
Syntaxin-18_N domain-containing protein	LSTR_LSTR010250	*Laodelphax striatellus* (Small brown planthopper)	592	1.2e-73	84.8%
Syntaxin-18	LOC113206671	*Frankliniella occidentalis* (Western flower thrips)	389	5.5e-43	55.3%
Syntaxin-18	LOC117645162	*Thrips palmi* (Melon thrips)	388	3.5e-43	59.8%
t-SNARE coiled-coil homology domain-containing	N/A	*Rhodnius prolixus* (Triatomid bug)	378	2.4e-41	51.4%

protein Syntaxin-18	STX18	*Blattella germanica* (German cockroach)	372	1.1e-40	61.2%

Table 2. Insect STX18 homologues retrieved from BLASTx and BLASTn.

BLASTx							
Hit	Organism	Accession	Max score	Total score	Query coverage	E value	% identity
Syntaxin-18	*Nilaparvata lugens* (brown planthopper)	XP_022191453.1	248	347	79%	1e-76	64.76
Hypothetical protein LSTR_LSTR010250	*Laodelphax striatellus* (small brown planthopper)	RZF32764.1	241	345	79%	3e-74	63.44
Unnamed protein product	*Timema cristinae* (stick insect)	CAD740252 9.1	133	194	73%	1e-39	52.78
Hypothetical protein Cfr_07670	*Coptotermes formosanus* (Formosan subterranean termite)	GFG34406.1	148	206	79%	4e-38	43.30
Syntaxin-18	*Blatella germanica* (German cockroach)	PSN44400.1	151	214	79%	3e-39	41.99
BLASTn							
Syntaxin-18	*Nilaparvata lugens* (brown planthopper)	LOC111049 633	614	614	86%	5e-171	80.74

N. lugens and *L. striatellus*, commonly known as brown planthopper and small brown planthopper, respectively, are also Hemipteran insects of the family Delphacidae which explains the high similarities with *P. maidis* in the sequences obtained. *N. lugens* is a known vector of both the *Rice grassy stunt virus* (RGSV) and the *Rice rugged stunt virus* (RRGV) while *L. striatellus* transmits *Rice stripe virus* (RSV), *Rice black-streaked dwarf virus* (RBSDV), *Barley yellow striate mosaic virus* (BYMSV), *Maize rough dwarf virus* (MRDV) and *Northern cereal*

mosaic virus (NCMV) and has been reported to have caused significant yield losses to the mentioned major hosts in the United States (Cabauatan et al., 2009; Mackesy & Moylett, 2018). *F. occidentalis* is commonly known as Western flower thrips native to western North America in the 1960s until its spread in the following decades to Asia, Africa and to other parts of North America. Plant viruses transmitted by *F. occidentalis* include *Tomato spotted wilt virus* (TSWV), *Tomato chlorotic spot virus* (TCSV), *Impatiens necrotic spot virus* (INSV) and *Groundnut ringspot virus* (GRSV) (Cluever et al., 2015). *T. palmi* causes economic damage to crops through direct feeding as well as from its ability to transmit tospoviruses such as *Groundnut bud necrosis virus*, *Mellon yellow spot virus* and *Watermelon silver mottle virus*. It is also speculated that melon thrips might be also a vector of another tospovirus, the *Tomato spotted wilt virus,* but this assumption is yet to be validated (Collins, 2016).

It is notable that most of the hits are STX18 or t-SNARE proteins from insects which are also known to be vectors or exhibits potential vector capacity. This suggests that *P. maidis* and the homologues share a common ancestry regarding STX18 and that the receptor may also be involved in viral transmission to their respective hosts.

Physicochemical properties and hydrophobicity of MMV G and PmStx18 provide insights into the stability of the predicted 3D structures

The proteins' physicochemical properties (**Table 3**) were calculated using the ProtParam tool of ExPASy. Based on the properties obtained, PmStx18 ($C_{832}H_{1331}N_{225}O_{286}S_3$) is composed of 170 amino acids weighing 19,158.94 Da. Thirty-one residues (Asp and Glu) are negatively charged while there are 14 positively charged amino acids (Arg and Lys). Amino acid composition showed that it has 21 glutamic acid residues accounting for 12.4%, followed by leucine, having 20 residues (11.8%) and 19 (11.2%) serine residues. On the other hand, MMV G ($C_{2962}H_{4542}N_{768}O_{880}S_{28}$), on the other hand, has 591 amino acid residues; 56 of them are negatively charged and 45 are positively charged. This protein is composed of 67 (11.3%) Serine residues, 49 (8.3%) isoleucine, 46 (7.8%) leucine as well as threonine residues.

The theoretical isoelectric points of PmStx18 and MMV G are 4.41 and 5.98, respectively. This implies that an interaction between the two proteins might be possible at this pH since there is reduced electrostatic forces and balanced positive and negative charges at pI (Novak et al., 2016). Calculated instability indexes shows that both are unstable *in vitro* since the values obtained are greater than the threshold value of 40 which indicates protein stability in a test tube (Gasteiger et al., 2007). Furthermore, MMV G contains lesser aliphatic amino acids than PmStx18 as evidenced by their aliphatic index values. Moreover, extinction coefficient was 2980 M-1 cm-1, which is the amount of light

PmStx18 can absorb at 280 nm measured in water. Calculated GRAVY values of both proteins are negative; thus, both were hydrophilic (Corredor et al., 2018).

Table 3. ProtParam calculations of the physicochemical properties of PmStx18 and MMV G protein sequences.

Properties	PmStx18	MMV G
Number of amino acids	170	591
Molecular weight (Da)	19158.24	65888.94
Theoretical pI	4.41	5.98
Total number of negatively charged residues (Asp + Glu)	31	56
Total number of positively charged residues (Arg + Lys)	14	45
Formula	$C_{832}H_{1331}N_{225}O_{286}S_3$	$C_{2962}H_{4542}N_{768}O_{880}S_{28}$
Total number of atoms	2677	9180
Extinction coefficients (M-1 cm-1, at 280 nm)	2980 2980	151105 150230
Estimated half-life	30 hours (mammalian reticulocytes, *in vitro*), >20 hours (yeast, in vivo) >10 hours (*Escherichiacoli*, in vivo)	30 hours (mammalian reticulocytes, *in vitro*) >20 hours (yeast, in vivo) >10 hours (*Escherichia coli*,in vivo)
Instability index	72.13	42.36
Aliphatic index	91.24	86.07
Grand average of hydropathicity (GRAVY)	-0.504	-0.106

Furthermore, the hydrophobicity of PmStx18 and MMV G were illustrated using Kyte & Doolittle hydrophobicity scales from ProtScale shown in **Figure 1**. As shown, regions having positive values are hydrophobic (Vej & Denmark, 2005). These hydrophobic regions influence the folding of the proteins as well as provide hydrophobic interactions which contribute to the stability of the proteins' tertiary structures (Dyson et al., 2006; Lodish et al., 2000).

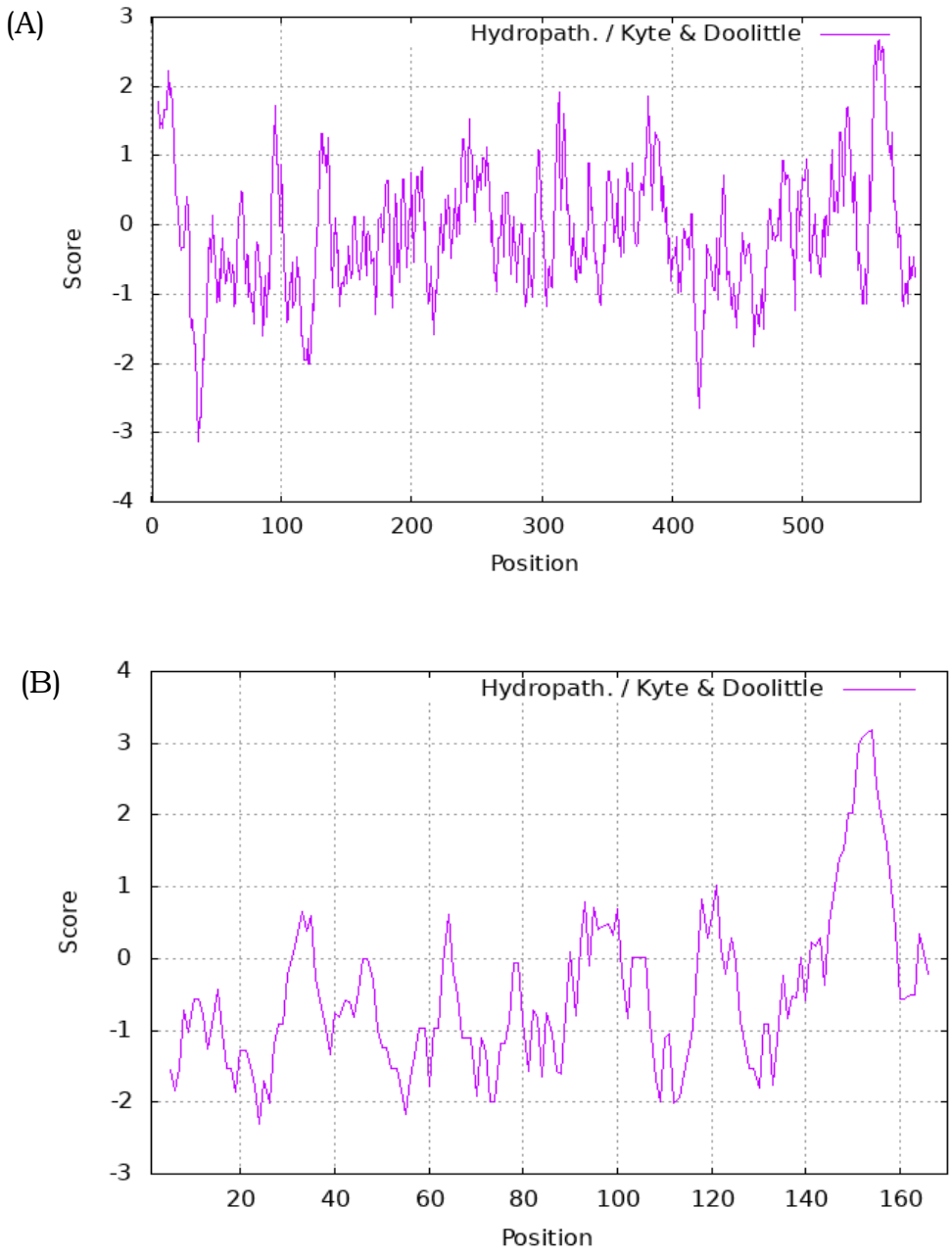

Figure 1. Kyte & Doolittle hydrophobicity scales of PmStx18 (A) and MMV G (B) protein sequences predicted using ProtScale tool.

Signal peptide (SP) and protein domains prediction show functional domains relevant to PPI of MMV G and PmStx18

SP identification plots (**Supplementary Figure 1**) for both PmStx18 and

MMV G obtained from SignalP 5.0 server showed a 21 amino acid-long signal sequence in MMV G. This may explain a possible function of the said protein in viral transmission since according to Singh et al. (2013), signal sequences are involved in the targeting and insertion of secretory and membrane proteins in both eukaryotes and prokaryotes.

The domain prediction plots for the two proteins (**Figure 2**) were from InterPro. Domain localization revealed that PmStx18 have the SNARE fusion complex from amino acids 73-140, the cytoplasmic domain at 1-144, the non-cytoplasmic domain from 163-170 and transmembrane domain at 145-162. Predicted disorder region cover 1-56 and coils are from 65-99 (yellow green line) (**Figure 2A**).

MMV G domains localization in InterPro has also detected SP presence having an N-region from amino acids 1-5, H-region from 6-17 and C-region from 18-21. The non-cytoplasmic domain is located at 22-550, cytoplasmic domain is from 574-591 and transmembrane region was predicted to be located at 551-573 (**Figure2B**). **Figure 2C** and **2D** show the schematic representations of the domains of PmStx18 and MMV G, respectively, based on the plots from InterPro.

3D structures of PmStx18 and MMV G and its docked structures prediction show stable interaction

Both PmStx18 and MMV G protein sequences were submitted to I-TASSER to predict the three-dimensional structures. ITASSER provided ten structural analogues of the query protein from the Protein Data Base (PDB) ranked from the highest TM-score to the lowest. These analogue proteins are also provided RMSD, percent identity as well as coverage.

The protein which is the most structurally close to the top 3D model of PmSTX18 (**Supplementary Table 1**) is a de novo-designed two-domain protein having a 0.935 TM-score, followed by anaphase-promoting complex sub-unit 1 which is involved in chromosome segregation and mitotic exit. The third analogue is PBI1, a protein which interacts with an ubiquitin ligase in rice for immunity, followed by an invasion protein from *C. violaceum*. The other analogues are classified as signaling protein (Methyl-accepting chemotaxis protein I), membrane protein (YaxA), protein binding (Methyl-accepting chemotaxis protein II) as well as structural protein (Flagellar hook-associated protein 3).

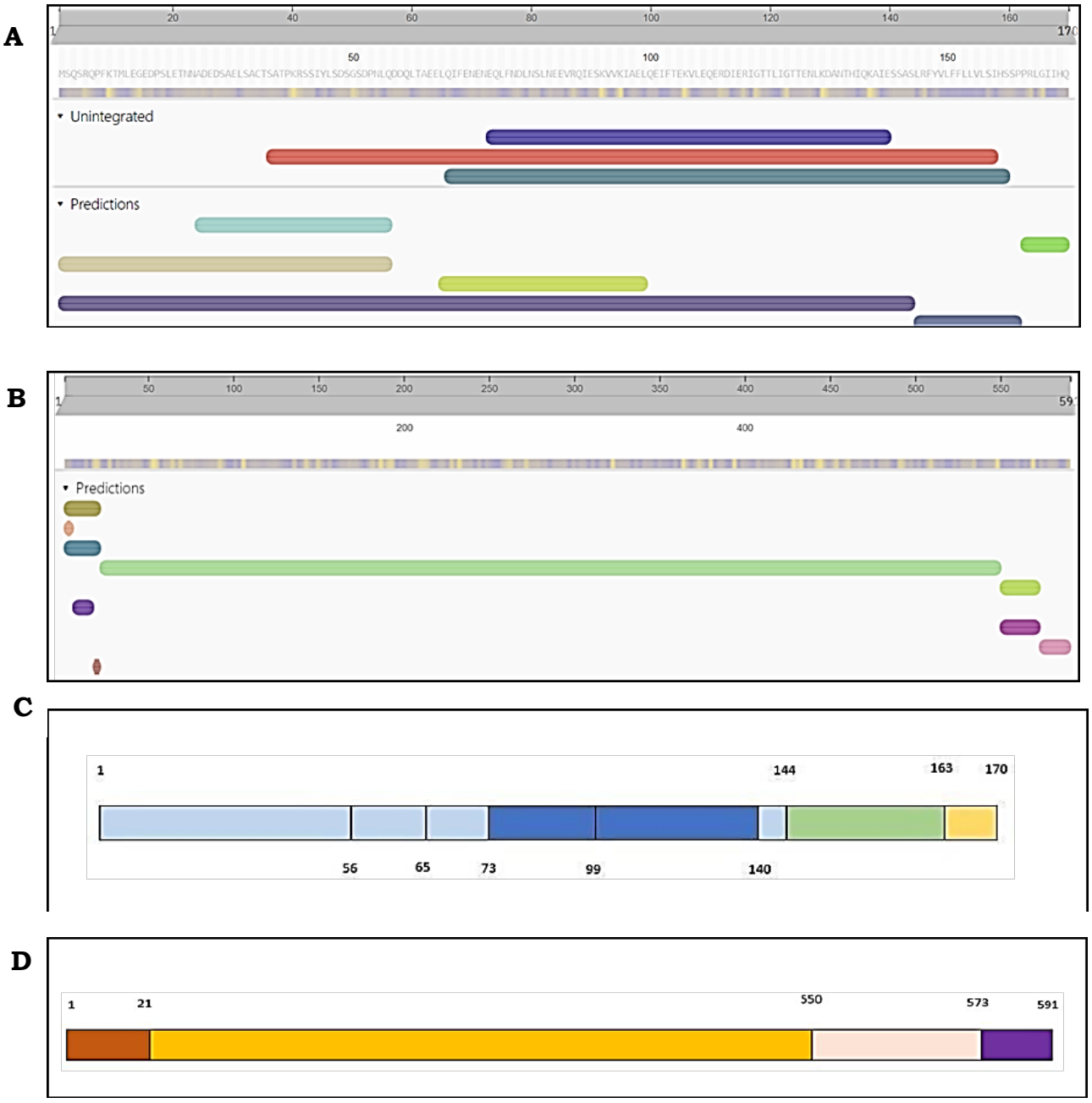

Figure 2. Results of protein domain prediction for PmStx18 **(A)** and MMV G **(B)** using InterPro and schematic representations showing the predicted domains, **(C)** PmStx18 with a length of 170 amino acids has cytoplasmic domain (1-144) with disordered regions (1-56) and coils (65-99), SNARE fusion complex (73-140), transmembrane domain (145-162), and non-cytoplasmic domain (163-170), **(D)** MMV G has a length of 591 amino acids with signal peptide (1-21), non-cytoplasmic domain (22-550), transmembrane domain (551-573) and cytoplasmic domain (574-591).

For the MMV G (**Supplementary Table 2**), its top-ranked analogue is a hydrolase from *S. cerevisiae*, followed by a membrane protein from the same organism. Some of the analogues are classified as membrane protein (V-type proton ATPase subunit A and V-type ATP synthase alpha chain), motor protein (V-type proton ATPase subunit A), hydrolase (V-type proton ATPase catalytic subunit A, V-type ATP synthase alpha chain and V-type proton ATPase subunit D), and sugar binding protein (Glycogen debranching enzyme).

To show the structural similarities of the PmSTX18 and its analogues, the predicted 3D model is superimposed on the analogue proteins (**Supplementary Figure 2**). Similarly, MMV G and its analogues are superimposed as presented in **Supplementary Figure 3**.

The server predicted five 3D models provided with confidence scores (C-score), an estimated template modelling score (TM-score) and an estimated root mean square deviation (RMSD) value. According to Zhang (2008), the C-score is calculated based on the significance of threading template alignments with values ranging from [-5, 2] where a C- score greater than -1.5 signifies a model of correct topology. The predicted models are ranked according to their C-scores and was the basis for choosing the appropriate structure. PmStx18 and MMV G structures are shown in **Figure 3**.

Based on the C-score cutoff value, both the generated models of PmStx18 and MMV Ghave the best quality among the given models as indicated by their C-score values of -1.11 and -1.32, respectively. Both protein models have an estimated TM-score of 0.55±0.15. PmSTX18 has an estimated RMSD of 7.9±4.4 Å and that of MMV G is 10.9±4.6 Å.

The ligand binding sites predicted by the ITASSER server are also ranked according to their C-scores which ranges from 0 to 1, whereas, a prediction having higher C-score value is more reliable. The ligand binding sites of both PmStx18 and MMV G are presented in **Tables 4** and **5**, respectively.

The proteins' top structures obtained from I-TASSER were submitted to HADDOCK 2.4 for the prediction of their docked models. Additionally, the predicted ligand binding residues for each of the proteins from I-TASSER were also submitted since these will serve as the putative interacting sites for subsequent protein-protein docking. A recent study reported the presence of a common PPI module, the PDZ-domain ligand binding site motif, in G-interacting *P. maidis* receptors which may interact with the PDZ-binding motif of MMV G (Alviar et al., 2022 Preprint). However, further analysis is needed to determine if the ligand binding sites obtained from ITASSER are residues from said domain.

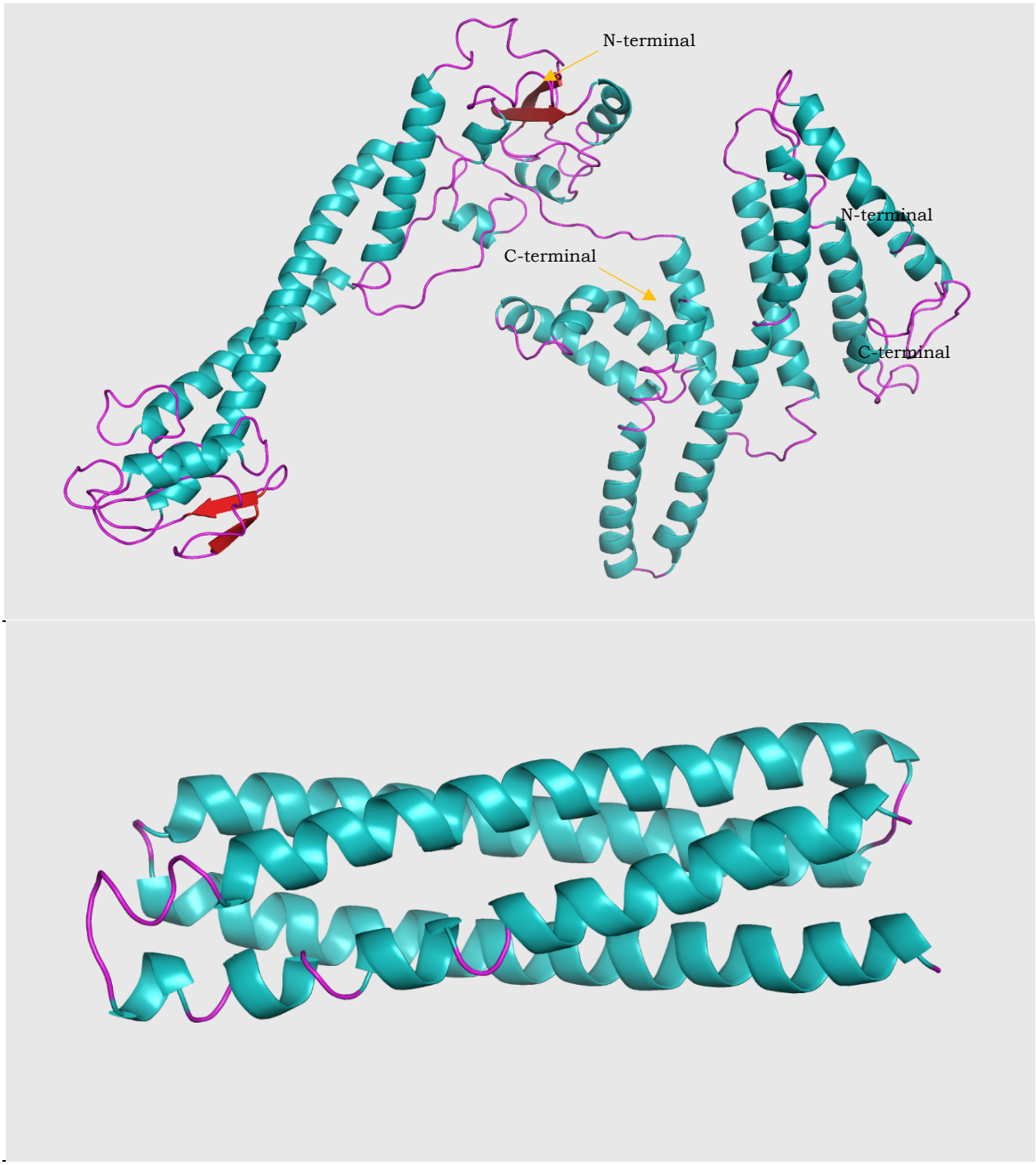

Figure 3. Three-dimensional models of MMV G (A) and PmStx18 (B) predicted in I-TASSER

Table 4. Predicted ligand binding sites of PmStx18 retrieved from I-TASSER.

Rank	C-score	Cluster size	PDB hit	Ligand name	Ligand binding sites residue
1	0.08	8	4d6tC	HEM	18, 21, 22, 25, 26, 28, 58, 61, 62, 65, 107, 108, 111, 112, 114, 115, 146, 147, 150
2	0.07	7	2dyrC	CDL	19, 22, 30, 147, 150, 151
3	0.05	5	4pv1A	CLA	114, 115, 118, 142, 146
4	0.04	4	4w8pA	PEPTIDE	62, 63, 66, 70, 73, 74, 77, 94, 97, 98, 101, 104, 108, 112
5	0.04	4	3l74C	HEM	28, 29, 32, 33, 35,

Table 5. Predicted ligand binding sites of MMV G retrieved from I-TASSER.

Rank	C-score	Cluster size	PDB hit	Ligand Name	Ligand Binding Site residues
1	0.05	2	5czdA	1N2	161, 290, 293, 294, 329, 482, 530, 531
2	0.05	2	3ko0B	TFP	185, 189
3	0.05	2	3tzzB	XPM	161, 247,251, 290, 329, 332, 333, 391, 475, 477, 480, 482, 485, 486, 488
4	0.05	2	4bhvA	CA	318, 321
5	0.05	2	2jfkB	COA	460, 473

Scoring functions were provided for the top four clusters as basis for ranking. Prediction of docked complexes used the easy interface of the web server and any other parameters were on default.

Statistics of the structures were showed in **Table 6**. The four models from Cluster 1 obtained a HADDOCK score of -139.2 +/-7.1, a cluster size of 23, RMSD from the overall lowest-energy structure of 5.5 +/-0.4, Van der Waals energy of -49.8 +/- 5.2, electrostatic energy of -319.4 +/-14.8, desolvation energy of -36.4 +/-4.8, restraints violation energy of 108.8 +/-50.1, buried surface are of 2086.6 +/- 119.2 and a Z-score of -1.5. Among the four clusters presented, Cluster 1 gave the most stable protein-protein interaction docked structures for

PmStx18 and MMV G.

Table 6. Scoring of the top four clusters of docked structures from HADDOCK 2.4.

Statistics	Cluster 1	Cluster 9	Cluster 5	Cluster 3
HADDOCK score	-139.2 +/- 7.1	-135.9 +/- 17.7	-135.0 +/- 3.8	-123.3 +/- 7.8
Cluster size	23	5	13	15
RMSD from the overall lowest-energy structure	5.5 +/- 0.4	0.6 +/- 0.4	0.8 +/- 0.3	18.0 +/- 0.1
Van der Waals energy	-49.8 +/- 5.2	-60.1 +/- 6.2	-58.4 +/- 3.1	-60.3 +/- 6.2
Electrostatic energy	-319.4 +/- 14.8	-192.7 +/- 26.6	-222.1 +/- 18.1	-195.6 +/- 13.8
Desolvation energy	-36.4 +/- 4.8	-54.4 +/- 5.5	-47.5 +/- 2.5	-35.2 +/- 2.8
Restraints violation energy	108.8 +/- 50.1	171.3 +/- 59.0	153.3 +/- 17.0	113.1 +/- 24.1
Buried surface area	2086.6 +/- 119.2	2300.9 +/-149.5	2271.6 +/- 73.0	2380.6 +/-152.2
Z-score	-1.5	-1.2	-1.2	-0.3

The top four docked structures of the best predicted cluster (Cluster 1) were retrieved (**Figure 4**) as follows. The interacting residues between the two proteins are presented in **Table 7**. **Figure 4A** shows the top predicted docked structures of MMV G (red ribbon) and PmStx18 (blue ribbon) of Cluster1 with 45 interacting residues. Similarly, **Figure 4B** shows the second docked structure of MMV G (green ribbon) and PmStx18 (red ribbon) with 42 interacting residues. Figures 4C (MMV G in green and PmStx18 in pink) and 4D (MMV G in brown and PmStx18 in blue) are the third and fourth best structures having 22 and 27 interacting residues, respectively.

Analysis of the theoretical pI of interacting residues supports fusion events of MMV G similar to other rhabdoviruses

The sequences (in one-letter amino acid name format) of the interacting residues of PmStx18 and MMV G from each of the four docked complexes were submitted to ExPASy Compute pI/MW (https://web.expasy.org/compute_pi/) and Isoelectric Point Calculator (http://isoelectric.ovh.org) to compute the pI of the interacting protein surface. The calculated theoretical isoelectric points of the four models of Cluster 1 were shown in **Table 8**. As shown in the table, the pI of the interacting sequences of PmStx18 in models 1 and 4, with model 4 having

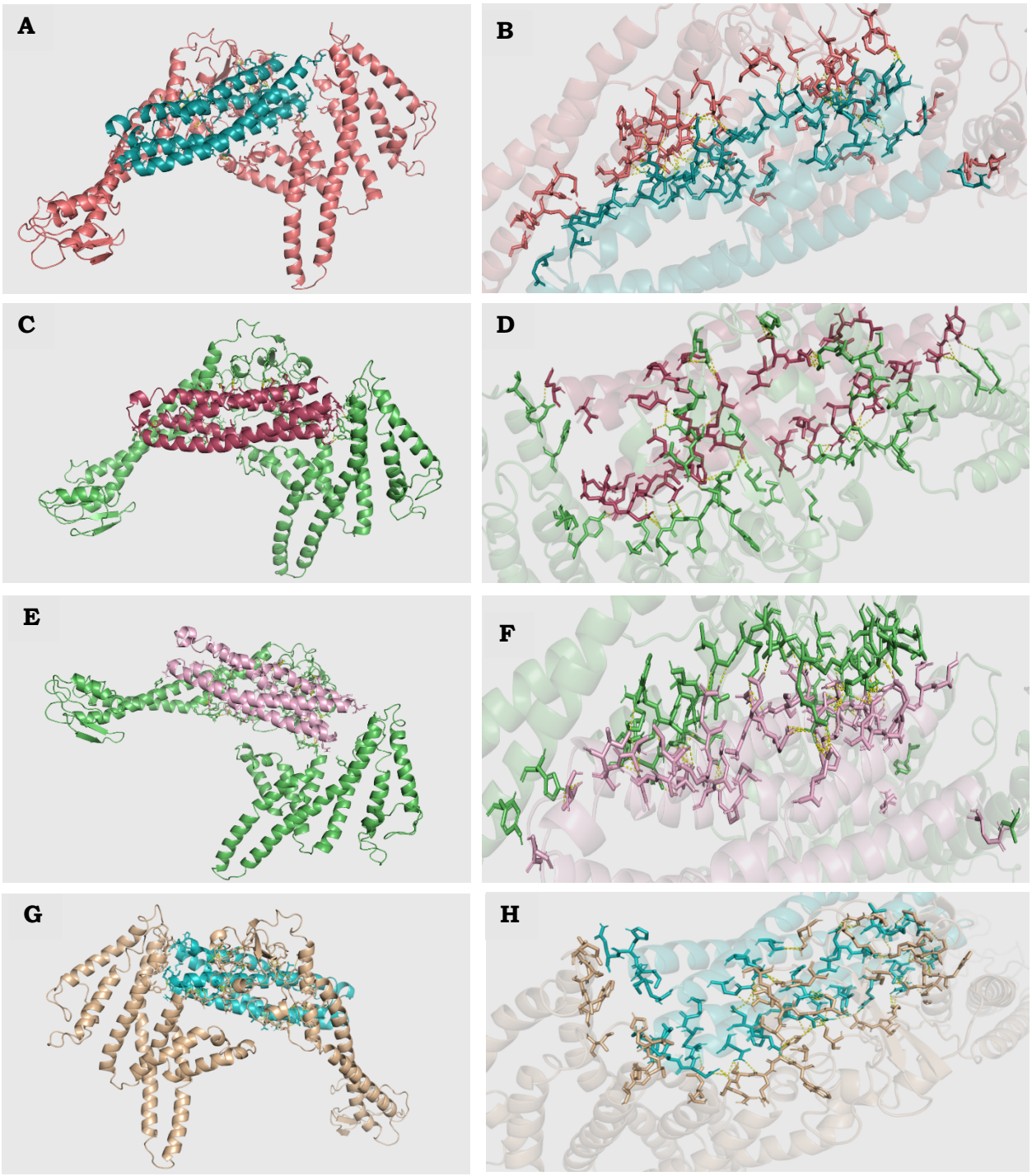

Figure 4. Docked structures (A, C, E, F) of PmStx18—MMV G interaction from Cluster 1 predicted in HADDOCK 2.4. (A) PmStx18 (blue)—MMV G (cyan red) top generated docked complex. (B) PmStx18 (red)—MMV G (green) second generated docked complex (C) PmStx18 (pink)—MMV G (cyan green) third generated docked complex (D) PmStx18 (blue)—MMV G (brown) fourth generated docked complex.

The corresponding magnified residues interaction of PmStx18—MMV G are also shown (B, D, F, H).

Table 8. Theoretical pI of the interacting residues of the docked complexes calculatedusing ExPASy Compute pI/MW and Isoelectric Point Calculator.

	STX18		MMV G	
Docked structures	ExPASy Compute	Isoelectric point calculator	ExPASy Compute	Isoelectric point calculator
	pI/MW		pI/MW	
Model 1	5.51	5.34	4.30	4.16
Model 2	6.44	6.71	12.78	12.62
Model 3	9.19	9.08	7.02	7.44
Model 4	5.22	5.03	10.00	9.24

the lowest computed pI, are relatively low compared with models 2 and 3 complexes. For the MMV G, the lowest calculated pI is observed in the MMV G interacting residues of model 1 and highest in model 2. It could also be said that most of the MMV G interacting residues in models 2 and 4 are comprised of mostly basic amino acids as evidenced by the high theoretical pI. More importantly, considering the identifiedinteracting sites in each docked complex, model 1 has 45 interacting residues, 42 residuesfor model 2, 22 residues for model 3 and 27 for model 4. This now implies that at an acidic pH, such that of the first model, more amino acids are likely to interact. In connection with the theoretical pI of interactingresidues, fusion might also be observed at an acidic pH. The entry and fusion of virus intohost cells since rhabdoviruses such as *Rabies virus* (RABV) and *Vesicular stomatitis virus*(VSV) are pH-dependent when it comes to these processes (Gaudin, 2000; Blumenthal et al., 1987). RABV glycoprotein (RABV G) undergoes structural transitions at low pH to mediate membrane fusion and this might be the same for MMV G might undergo conformational changes at certain pH. This implies that MMV G might also assume three states the same way RABV G re-orients at low pH. The three conformation states are: the native (N) state, activated (A) hydrophobic state, and the fusion inactive (I) conformation (Gaudin, 2000).

Additionally, MMV fusion events might also be in line with the pH-dependent fusion observed in VSV with plasma membrane of Vero cells at pH below 6 shown through dequenching of octadecyl rhodamine fluorescence (Blumenthal et al., 1987). Another studyfurther showed the same concept using *Chandipura virus* (CHAV), a member of the genus *Vesiculovirus* associated with

encephalitis in India, revealed that, its entry via recognition and fusion of its envelope glycoprotein with host cells is very similar with that of VSV G which could be triggered at pH below 6.5 (Baquero et al., 2015).

Binding affinities (ΔG) of MMV G and PmStx18 provides understanding of the stability of the interaction

The extent of association of a protein with a ligand is determined by the magnitude of the negative ΔG and is considered as the measure of stability or binding affinity of any protein-ligand complex since like any spontaneous process, interaction of protein and ligand only occurs when the change in Gibbs free energy is negative and that, a more negative ΔG value indicates more sites that are interacting (Du et al., 2016). The binding affinities of the docked complexes obtained in PRISM are shown in **Table 9**.

Table 9. Binding affinities of docked the structures obtained from PRISM.

PDB 1	PDB 2	Interface	Energy (ΔG)
Syntaxin-18	MMV G	2ehoGH	-57.73
		3ct6AB	-57.05
		3ct6AB	-52.55
		3ct6AB	-51.69

In silico prediction of PPI showed that residues from the SNARE fusion complex, cytoplasmic domain, and transmembrane domain of PmStx18 interact with residues from the non-cytoplasmic domain of MMV G. Prediction of contact of interface residues further revealed that the domains involved in the interaction are located on chain A of both proteins. Furthermore, the properties of the projected docked complexes such as the interacting residues could be considered as accurate since these binding residues are on par with the ligand binding sites predicted at the individual protein level.

Moreover, the predicted interaction of PmStx18 and MMV G is further supported by the binding affinity values since, according to Bronowska (2011), binding occurs only when it is associated with a negative Gibbs free energy of binding. More importantly, Kamal et al. (2019) reported that the binding affinity measured through change in Gibbs free energy score indicates interaction between proteins since a more negative free energy is directly proportional to a more stable protein complex. This also indicate that there is stability in the interaction of the proteins among the four docked complexes, with the top structure being the most stable as evidenced by the lowest value of Gibbs free energy.

The interaction of PmStx18 with MMV G suggests that this vector protein might be involved in mediating the viral infection and replication within the *P. maidis*. Previous studies on similar t-SNARE protein revealed the interaction of STX18 with the minor capsid protein L2 of *Bovine papillomavirus type 1* (BVP1) (Bossis et al., 2005). BVP1 belongs to the genus *Papillomaviruses* and are reported causative agents of lesions in squamous epithelial cells, mostly in higher vertebrates (Bossis et al., 2005). Bossis and colleagues demonstrated the interaction by using BVP1 which exhibits mutated conserved domain in the protein L2. The changes made on the conserved domain of L2 protein resulted to failure in its interaction with STX18, thus, non-infection occurred. This was further proven by the study of Laniosz et al. (2007) where they also investigated the association of BPV1 capsid L2 and STX18 and obtaining similar results.

Earlier studies regarding the roles of STX18 disclosed that it functions in the transport between the endoplasmic reticulum and Golgi complex, specifically in the exocytic and endocytic pathways (Hatsuzawa et al., 2000). In this regard, the dissemination of MMV within *P. maidis* previously described by Ammar & Hogenhout (2008) could be through the said processes. The insect midgut, which has been reported as the first barrier to viral acquisition as well as the initial infection site is lined with epithelial cells (Qin et al., 2008). The study of Qin et al. (2008) revealed that the interaction of the nucleocapsid protein (NP) of the *Rice stunt virus* (RSV) with a highly expressed protein in the midgut of delphacid planthopper *Laodelphax striatellus*, sugar transporter 6 (ST6) mediates the entry of RSV into the midgut epithelial cells of its vector. In line with this, the entry of RSV into *L. striatellus* through the NP-ST6 docking suggest that the same mechanism might be employed in overcoming the initial barrier in the entry as well as further spread of MMV particles within *P. maidis*. The movement of the virus to anterior diverticulum and/or esophagus might follow the findings of Hatsuzawa et al. (2006) which could be through ER-mediated phagocytosis as it was demonstrated that STX18 is involved in regulating the specific and direct fusion of ER and plasma or phagosomal membranes in murine J774 macrophages.

Virus dissemination spreads through the nervous system of *P. maidis* following successful entry and invasion of the anterior diverticulum and esophagus (Ammar & Hogenhout, 2008). In line with this, further infection of MMV in the tissues of the vector's nervous system via interaction with PmStx18 might be due to the fusion events occurring in the nerves as several studies have proven that SNAREs are involved in vesicle fusion for neurosecretion as well as neurotransmitter release in neuronal cells (Ramakrishnan et al., 2012).

Like any other Rhabdovirus, the entry and infection of MMV into *P. maidis* cells could be through the clathrin-mediated endocytosis (CME) pathway since commonly known and studied viruses from the family *Rhabdoviridae* such as RABV demonstrated that viral entry is through the said pathway facilitated by low pH fusion of the endosomesduring early stages of RABV infection (Guo et al., 2019; Picinotti et al., 2013). Furthermore, the uptake of host cell of VSV was also confirmed by clathrin knockdown using small interfering RNA (siRNA duplexes) (Sun et al., 2004). In addition, another rhabdovirus, the *Australian bat lyssavirus* (ABLV) employ the same mechanism which was reported by Weir et al. (2014) to enter host cells via CME and subsequent low pH fusion. Similarly, the *Infectious hematopoietic necrosis virus* (IHNV) of the genus *Novirhabdovirus* is a rhabdoviral fish pathogen infecting wild and cultured salmonids was found out to have reduced viral entry with treatment of chlorpromazine, a drug which inhibits CME suggesting that its entry is CME dependent (Liu et al., 2011).

The PmStx18—MMV G interaction further highlights the capability of *P. maidis* in transmitting MMV as previous studies regarding the vector-pathogen relationship have revealed its efficiency in vectoring viruses. The study of Alviar et al. (2016) have disclosed the acquisition efficiency of the insect, where nymphs are more efficient at acquiring the virus than adults. More so, the vector's efficiency is evidenced by the viral replication that occurs throughout the life span of *P. maidis* once acquired (Alviar et al., 2016).

SUPPLEMENTARY MATERIALS

Supporting information can be downloaded at: https://TPESupplementaryMaterial.

ACKNOWLEDGEMENT

KBAlviar acknowledges the National Research Council of the Philippines of the Department of Science and Technology (Fund Code 101) for the project grant that supported part of the research activities of ANClemente.

REFERENCES CITED

ABBAS MT, SHAFIQ M, ARSHAD H, HAROON R, MASQOOD H, HAIDER MS. 2022. Viral diseases of maize. In: Abd-Edsalam KA, Mohamed HI (Eds.) Cereal diseases: Nanobiotechnological approaches for diagnosis and management. Springer, Singapore.

ALVIAR KB, ROTENBERG D, MARTIN KM, WHITFIELD AE. 2022. Identification of interacting proteins of maize mosaic virus glycoprotein in its vector, *Peregrinus maidis* (Preprint). doi: https://doi.org/10.1101/2022.02.01.478665.

ALVIAR KB, RAMIREZ GM, ROTENBERG D, WHITFIELD AE. 2016. Analysis of acquisition and titer of Maize mosaic rhabdovirus in its vector, *Peregrinus maidis* (Hemiptera: Delphacidae). Journal of Insect Science 16(1): 14; 1-8.

AMMAR E, HOGENHOUT SA. 2008. A neurotropic route for maize mosaic virus (Rhabdoviridae) in its planthopper vector *Peregrinus maidis*. Virus Research 131 (1): 77–85.

BACKOVIC M, JARDETZKY TS. 2011. Class III viral membrane fusion proteins. Advances in Experimental Medicine and Biology 714:91-101.

BARANDOC-ALVIAR, K., BADILLO-VARGAS, I.E. AND WHITFIELD, A.E., 2016. Interactions between insect vectors and propagative plant viruses. In: Czosnek H, Ghanim M. (Eds). Management of insect pests to agriculture. (pp. 133-180). Springer, Cham.

BAQUERO E, ALBERTINI AA, RAUX H, BUONOCORE L, ROSE JK, BRESSANELLI S, GAUDIN Y. 2015. Structure of the low pH conformation of Chandipura virus G reveals important features in the evolution of the Vesiculovirus glycoprotein. PLOS Pathogens 11(3).

BLUMENTHAL R, BALI-PURI A, WALTER A, COVELL D, EIDELMAN O. 1987. pH-dependent fusion of Vesicular stomatitis virus with Vero cells. Journal of Biological Chemistry 262(28): 13614-13619.

BOSSIS I, RODEN RBS, GAMBHIRA R, YANG R, TAGAYA M, HOWLEY PM, MENESES PI. 2005. Journal of Virology 79 (11): 6723–31.

BRONOWSKA, AK. 2011. Thermodynamics of ligand-protein interactions: Implications for molecular design. In Moreno-Pirajan, JC (Ed). Thermodynamics-Interaction studies- Solids, Liquids and Gases. Chapter 1.

CABAUATAN, PQ, CABUNAGAN, RC, CHOI, I. 2009. Rice Viruses transmitted by the brown planthopper *Nilaparvata lugens* Stål. In: K.L. Heong, and B. Hardy editors, Planthoppers: New Threats to the Sustainability of Intensive Rice Production Systems in Asia. International Rice Research Institute, Los Baños, Philippines. pp. 357–68.

MELVIN A. CASTROSANTO MA, APEL JAE N. CLEMENTE AJN, ANNA E. WHITFIELD AE, ALVIAR KB. 2022. In silico analysis of the predicted protein-protein interaction of syntaxin-18, a putative receptor of *Peregrinus maidis* Ashmead (Hemiptera: *Delphacidae*) with Maize mosaic virus glycoprotein. Journal of Biomolecular Structure and Dynamics. doi: 10.1080/07391102.2022.2059569.

CLUEVER JD SMITH HA, FUNDERBURK JE, FRANTZ G. 2015. Western flower thrips (*Frankiniella occidentalis* [Pergande]). IFAS Extension, University of Florida. Accessed July 23, 2021 at https://edis.ifas.ufl.edu/publication/IN1089.

COLLINS D. 2016. Melon thrips. Plant Pest Factsheet. Department for Environment, Food and Rural Affairs. Accessed July 23, 2021 at https://planthealthportal.defra.gov.uk/assets/factsheets/thrips-palmi-factsheet.pdf.

CORREDOR AP, GONZALEZ J, BAQUERO LA, CURTIDOR H, OLAYA-GALAN NN, PATARROYO MA, GUTIERREZ MF. 2018. *In silico* and *in vitro* analysis of boAP3d1 protein interaction with bovine leukemia virus gp51. PLoS ONE 13(6): e0199397.

DIETZGEN RG, MANN KS, JOHNSON KN. 2016. Plant virus-insect vector interactions: Current and potential future research directions. Viruses 8(11): 303.

DU X, LI Y, XIA Y, AI S, LIANG J, SANG JP, JI X, LIU A. 2016. Insights into protein-ligand interactions: Mechanisms, models, and methods. International Journal of Molecular Science 17(144).

ERENSTEIN O, JALETA M, SONDER K, MOTTALEB K, PRASANNA BM. 2022. Global maize production, consumption and trade: trends and R&D implications. Food Security 14: 1295-1319.

DYSON HJ, WRIGHT PE, SCHERAGA HA. 2006. The role of hydrophobic interactions in initiation and propagation of protein folding. Proceedings of National Academy of Sciences of the United States of America103(35): 13057-13061.

FAROOQ QUA, SHAUKAT Z, AIMAN S, LI CH. 2021. Protein-protein interactions: Methods, databases, and applications in virus-host study. World Journal of Virology10(6): 288-300.

GASTEIGER E, HOOGLAND C, GATTIKER A, DUVAUD S, WILKINS MR, APPEL RD, BAIROCH A. 2007. Protein identification and analysis tools on the ExPASy server. The Proteomics Protocols Handbook. JM Walker (Ed.)

Humana Press Inc, Totowa, NJ.

GAUDIN Y. 2000. Rabies virus-induced membrane fusion pathway. The Journal of Cell Biology 150(3): 601-611

GUO Y, DUAN M, WANG X, GAO J, GUAN Z, ZHANG M. 2019. Early events in rabies virus infection- attachment, entry, and intracellular trafficking. Virus Research 263: 217-225.

HATSUZAWA K, HIROSE H, TANI K, YAMAMOTO A, SCHELLER RH, TAGAYA M. 2000. Syntaxin-18, a SNAP receptor that functions in the endoplasmic reticulum. intermediate compartment, and cis-Golgi vesicle trafficking. Journal of Biological Chemistry 275(18):13713-13720.

HATSUZAWA K, TAMURA T, HASHIMOTO H, HASHIMOTO H, YOKOYA S, MEGUMI M, NAGAYA H, WADA I. 2006. Involvement of Syntaxin-18, an endoplasmic reticulum (ER)-localized SNARE protein, in ER-mediated phagocytosis. Molecular Biology of the Cell 17: 3964-3977.

HOGENHOUT, S.A., AMMAR, E.D., WHITFIELD, A.E. AND REDINBAUGH, M.G., 2008. Insect vector interactions with persistently transmitted viruses. Annual Review of Phytopathology 46:327-359.

HOLZ RW, ZIMMERBERG J. 2019. Dynamic relationship of the SNARE complex with a membrane. Biophysical Journal. 117 (4): 627–30.

INTERNATIONAL COMMITTEE ON TAXONOMY OF VIRUSES. 2020. Genus: Alphanucleorhabdovirus. Accessed July 1, 2021 at talk.ictvoline.org.

JOURDAN-RUF C, MARCHAND JL, PETERSCHMITT M, REYNAUD B, DINTINGER J. 1995. Maize streak, maize stripe and maize mosaic virus in the tropics (Africa and islands in the Indian Ocean). Maize Virus Diseases Dossier (Special Issue).

KAMAL H, MINHAS FA, FAROOQ M, TRIPATHI D, HAMZA M, MUSTAFA R, KHAN MZ, MANSOOR S, PAPPU HR, AMIN I. 2019. *In silico* predictions and validations of domains involved in *Gossypium hirsutum* SnRK1 protein interaction with cotton leaf curl Multan betasatellite encoded βC1. Frontiers in Plant Science 10.

KARAVINA, C. 2014. Maize streak virus: A review of pathogen occurrence, biology and management options for smallholder farmers. African Journal of Agricultural Research 9 (36): 2736–2742.

LANIOSZ V, NGUYEN KC, MENESES PI. 2007. Bovine papillomavirus type 1 infection is mediated by SNARE syntaxin18. Journal of Virology 81(14):7435-7448.

LIU H, LIU Y, LIU S, PANG D, XIAO G. 2011. Clathrin-mediated endocytosis in living host cells visualized through dot labeling of Infectious hematopoietic necrosis virus. Journal of Virology 85(13): 6252-6262.

LODISH H, BERK A, ZIPURSKY SL. 2000. Hierarchical structure of proteins. In: W.H. Freeman (Ed.) Molecular Cell Biology (4th edition), pp.81-109. New York. Accessed July 8, 2021 at ncbi.nlm.nih.gov.

MACKESY DZ, MOYLETT H. 2018. CPHST pest datasheet for *Laodedlphax striatellus* USDA-APHIS-PPQ-CPHST.

MUELLER DS, WISE KA, SISSON AJ, ALLEN TW, BERSTROM GC, BISSONNETTE KM, BRADLEY CA, BYAMUKAMA E, CHILVERS MI, COLLINS AA, ESKER PD, FASKE TR, FRISKOP AJ, HAGAN AK, HEINIGER, RW, HOLLIER CA, ISAKEIT T, JACKSON-ZIEMS TA, JARDINE DJ, KELLY HM, KLECZEWSKI NM, KOEHLER AM, KOENNING SR,MALVICK DK, MEHL HL, MEYER RF, PAUL PA, PELTIER AJ, PRICE PP, ROBERTSON AE, ROTH GW, SIKORA EJ, SMITH DL, TANDE CA, TELENKO DEP, TENUTA, AU, THIESSEN LD, WIEBOLD WJ. (2020). Corn yield loss estimates due to diseases in the United States and Ontario, Canada, from 2016-2019. Plant Health Progress 21: 238-247.

NOVAK P, HAVLICEK V. 2016. Protein extraction and precipitation. In: P. Ciborowski, Silberring J. (Eds) (Second Edition), Proteomic Profiling and Analytical Chemistry. Chapter 4: 51-62. Accessed July 8, 2021 at doi: 10.1016/B978-0-444-63688-1.00004-5.

PICCINOTTI S, KIRCHHAUSEN T, WHELAH SPJ. 2013. Uptake of rabies virus into epithelial cells by clathrin-mediated endocytosis depend on actin. Journal of Virology 82(21): 11637-11647.

QIN F, LIU W, WU N, ZHANG L, ZHANG Z, ZHOU X, WANG X. 2008. Invasion of midgut epithelial cells by a persistently transmitted virus is mediated by sugar transporter 6 in its vector. PLOS Pathogens. 14(7): e1007201.

RAMAKRISHNAN NA, DRESCHER MJ, DRESCHER DG. 2012. The SNARE complex in neuronal and sensory cells. Molecular and Cellular Neuroscience 50(1): 58-69.

RANUM P, PEÑA-ROSAS JP, GARCIA-CASAL MN. 2014. Global maize production, utilization, and consumption. Annals of the New York Academy of Sciences 1312:105-112.

ROCHE S, ALBERTINI AAV, LEPAULT J, BRESSANELLI S, GAUDIN Y. 2008. Structures of vesicular stomatitis virus glycoprotein: membrane fusion revisited. Cellular and Molecular Life Sciences 65: 1716-1728.

SHAH TR, PRASAD K, KUMAR P. 2016. Maize—A potential source of human nutrition and health: A review. In: Fatih Yildiz (Ed.). Cogent Food and Agriculture 2(1).

SINGH P, SHARMA L, KULOTHUNGAN SR, ADKAR BV, PRAJAPATI RS, ALI PSA, KRISHNAN B, VARADARAJAN R. 2013. Effect of signal peptide on stability and folding of *Escherichia coli* thioredoxin. PLoS ONE 8(5): e63442.

SRINIVASA RAO V, SRINIVAS K, SUJINI GN, SUNAND KUMAR GN. 2014. Protein-protein interaction detection: methods and analysis. International Journal of Proteomics. Volume 2014.

SUN PD, FOSTER CE, BOYINGTON JC. 2004. Overview of protein structural and functional folds. Current Protocols in Protein Science. Chapter 17(1): Unit 17.1. John Wiley & sons, Inc.

SUN T, ZHOU B, LAI L, PEI J. 2017. Sequence-based prediction of protein protein interaction using a deep-learning algorithm. BMC Bioinformatics 18 (277).

VEJ GW, DENMARK AC. 2005. Bioinformatics Explained: Hydrophobicity. Accessed August 16, 2021 at https://home.hiroshima-u.ac.jp/kei/IdentityX/picts/BE-hydrophobicity.pdf.

WANG T, LI L, HONG W. 2017. SNARE proteins in membrane trafficking. Traffic 18(12): 767–75. John Wiley & Sons. doi: 10.1111/tra.12524.

WEIR DL, LAING ED, WANG L, BRODER CC. 2014. Host cell virus entry mediated by Australian bat lyssavirus G envelope glycoprotein occurs through a clathrin- mediated endocytic pathway that requires actin and Rab5. Virology Journal 11(40).

WEISSENHORN W, HINZ A, GAUDIN Y. 2007. Virus membrane fusion. FEBS Letters. 581(11):2150-5.

WHITFIELD AE, HOUT OB, MARTIN KM, KONDO H, DIETZGEN RG. 2018. Plant Rhabdoviruses- their origins and vector interactions. Current Opinion in Virology 33: 198-207.

YANG F, LIN S, YE F, WEI Y, GAO GF, LU G. 2020. Structural analysis of Rabies virus glycoprotein reveals as pH-dependent conformational changes and interactionswith neutralizing antibody. Cell Host & Microbe (27): 441-453.

YOON TY, MUNSON M. 2018. SNARE complex assembly and disassembly. Current Biology. 28(8): 397-401.

ZHANG Y. 2008. I-TASSER server for protein 3D structure prediction. BMC Bioinformatics 9(40).